Triplet f-wave pairing in SrPtAs

Wan-Sheng Wang,[1] Yang Yang,[1,2] and Qiang-Hua Wang[1,3]
[1]*National Laboratory of Solid State Microstructures & School of Physics, Nanjing University, Nanjing, 210093, China*
[2]*College of Physics and Electronic Engineering, Zhenzhou University of Light Industry, Zhenzhou, 450002, China*
[3]*Collaborative Innovation Center of Advanced Microstructures, Nanjing 210093, China*
(Received 18 December 2013; revised manuscript received 4 September 2014; published 22 September 2014)

We constructed tight-binding models for the superconductor SrPtAs according to first principle calculations, and by functional renormalization group we investigated the effect of electron correlations and spin-orbital coupling (SOC) in Cooper pairing. We found that out of the five d orbitals, the (d_{xz},d_{yz}) orbitals are the active ones responsible for superconductivity, and ferromagnetic spin fluctuations enhanced by the proximity to the van Hove singularity triggers f-wave triplet pairing. The superconducting transition temperature increases as the Fermi level approaches the van Hove singularity until ferromagnetism sets in. Because of SOC, the spin fluctuations have easy-plane anisotropy, and the **d** vector of the triplet pairing component is pinned along the out-of-plane direction. Experimental perspectives are discussed.

DOI: 10.1103/PhysRevB.90.094514 PACS number(s): 74.20.Rp, 74.62.−c, 74.70.Xa

I. INTRODUCTION

Recently, SrPtAs was found to be a superconductor with a transition temperature $T_c \sim 2.4$ K [1]. This is a pnictide superconductor, but with a hexagonal lattice rather than the square lattice in iron pnictides. The difference in lattice geometry can lead to completely different electronic ground states. In square lattices, collinear spin magnetic order is generally realized (except for systems with ring exchanges), as in cuprates and iron pnictides [2,3]. However, a hexagonal lattice would lead to spin frustration, and even to ferromagnetism [4,5]. Since dynamic spin fluctuations can trigger unconventional superconductivity (SC), the difference in lattice geometry is expected to lead to novel SC. Interesting proposals have been made, e.g., for Na_xCoO_2 which also possesses a hexagonal lattice [6,7]. An even more profound aspect of SrPtAs is that the conducting element Pt is heavy, hence there is a significant atomic spin-orbital coupling (SOC) among the $5d$ orbitals. Such a coupling can break spin degeneracy (on general momentum points), modify the Fermi surface topology, and therefore modify low energy particle-hole excitation spectra. As a result, the effect of SOC is an indispensable factor for unconventional pairing. Moreover, the unit cell of SrPtAs contains two distinct PtAs layers, each of which has no inversion center, but the system has a global inversion symmetry with respect to the bisecting plane between the two layers. The lack of local inversion center opens the possibility of singlet-triplet mixing [8–10]. This is similar to the mixing in systems where even global inversion symmetry is absent [11–13]. Combined with strong SOC, such superconductors can exhibit enhanced Pauli limiting fields and a nonvanishing spin susceptibility down to zero temperature [11,14–17]. Therefore SrPtAs provides a playground to explore properties of centrosymmetric superconductors with possible singlet-triplet mixing.

Previous local density functional (LDA) calculations for SrPtAs [18,19] show the system is quasi-two-dimensional. There are three pairs of spin-split Fermi surfaces due to SOC. Two of them are centered around the zone center, contributing about 30% of the total density of states (DOS) at the Fermi level. The remaining 70% comes from the third pair of spin-split Fermi surfaces encircling the K and K' points. A comprehensive symmetry analysis of the band-resolved pairing symmetry reveals that SrPtAs may possess some unconventional superconducting states, such as the A_{2u} state with a dominant f-wave component and the E_g state with a dominant chiral d-wave component [8]. Recently, a muon spin-rotation/relaxation (μSR) measurement for SrPtAs [20] suggests time-reversal symmetry breaking (TRSB) and a nodeless pairing gap. A nuclear magnetic resonance (NMR) experiment [21] revealed that the spin-lattice relaxation rate $1/T_1$ shows a Hebel-Slichter peak below T_c, but the peak is strongly suppressed in another NMR experiment [22]. Therefore the exact pairing symmetry is still unclear, let alone the pairing mechanism.

The situation motivates us to study the paring mechanism and pairing symmetry of SrPtAs at a microscopic level. For this purpose we construct effective tight-binding models according to LDA band structures. The correlation effects are handled by the singular-mode functional renormalization group (SM-FRG) [4,23–28]. The advantage of FRG is the capability to survey all electronic instabilities at the same time [29], and this has been applied with great success in the contexts of cuprates [30], iron-based superconductors [31], and more recently for topological SC in correlated systems [24]. As compared to the usual patch-FRG, our SM-FRG has the additional advantages that it respects momentum conservation exactly and is more straightforward to deal with orbital and spin degrees of freedom.

In this paper, we find that out of the five d orbitals, the (d_{xz},d_{yz}) orbitals are the active ones responsible for SC, and ferromagnetic spin fluctuations enhanced by the proximity to the van Hove singularity (VHS) triggers f-wave triplet pairing. The superconducting transition temperature increases as the Fermi level approaches the VHS until ferromagnetism sets in. Because of SOC, the spin fluctuations have easy-plane anisotropy, and the **d** vector of the triplet pairing component is pinned along the out-of-plane direction. Experimental consequences of the SC are discussed.

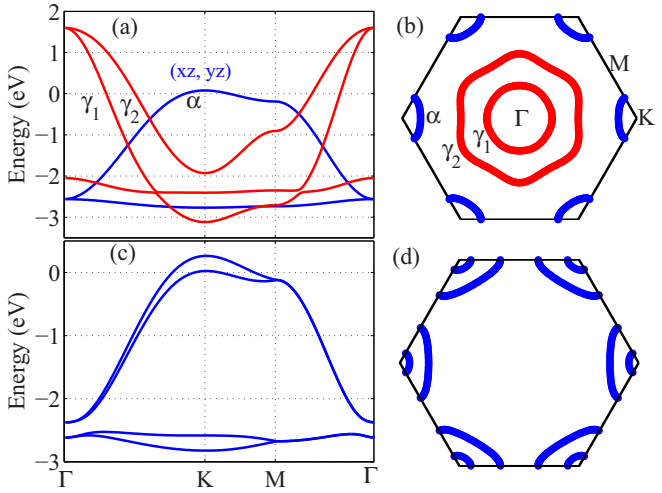

FIG. 1. (Color online) (a) and (b) are the spin-degenerate band structure Fermi surfaces for the five band model without SOC. (c) and (d) are spin-split band structure and Fermi surfaces for the two-orbital model with SOC.

II. MODEL AND METHOD

Figure 1(a) shows the spin-invariant band structure for SrPtAs obtained by using the Quantum-ESPRESSO package [32,33]. We then construct ten maximally localized Wannier functions [34] centered at the two Pt sites in the unit cell, each with five d orbitals $(d_{3z^2-r^2}, d_{xz}, d_{yz}, d_{x^2-y^2}, d_{xy})$. In agreement with the strong two-dimensionality found in previous LDA calculations, we find the interlayer coupling is weak. Thus we shall consider the one layer model (with one atom per unit cell) for brevity, and will come back to the effect of interlayer coupling before closing. The in-plane hopping integrals are presented in Table I. The orbital-dependent on-site energies are (7.577, 8.178, 8.178, 8.787, 8.787) eV, and finally the Fermi energy is $\mu = 9.915$ eV. We notice that although the lattice is hexagonal, the effect of As atoms lowers the point group symmetry to D_{3d}, and actually to C_{3v} in the effective one-layer model. The two pockets (labeled as γ_1 and γ_2) around the Γ point are derived from $(d_{3z^2-r^2}, d_{x^2-y^2}, d_{xy})$ orbitals, and the pockets around K and K' (labeled as α) are derived from (d_{xz}, d_{yz}) orbitals. The α pocket is close to the VHS at M and is expected to be more susceptible to correlation effects than the other pockets.

TABLE I. Hopping integrals $t_{\mu\nu}(\Delta)$ (in units of eV) where $\Delta = (\Delta_x, \Delta_y)$ denotes an in-plane hopping vector and (μ,ν) the orbitals. Combination of the C_{3v} symmetry and $t_{\mu\nu}(\Delta) = t_{\nu\mu}(-\Delta)$ produces all the in-plain hoppings up to the third neighbors. Here the five d orbitals $(d_{3z^2-r^2}, d_{xz}, d_{yz}, d_{x^2-y^2}, d_{xy})$ are labeled as (1,2,3,4,5) for brevity.

$(\mu,\nu)\backslash(\Delta_x,\Delta_y)$	(1,0)	$(0,\sqrt{3})$	$(0,-\sqrt{3})$	(2,0)
(1,1)	0.029	0.009	0.009	0.010
(1,4)	0.005	0	−0.018	0
(1,5)	0.022	0	0	0
(4,4)	0.158	0.043	0.043	−0.022
(4,5)	0.135	0	0	0.020
(5,5)	0.701	−0.050	−0.050	0.080
(2,2)	−0.456	0	0	−0.003
(2,3)	−0.277	0	0	−0.003
(3,3)	0.185	−0.005	−0.005	0.003

In order to judge the relative importance of the various orbitals, we first perform a SM-FRG study of the above five-orbital model in the absence of SOC. We assume standard local interactions with intraorbital repulsion U, interorbital repulsion U', Hund's rule spin exchange J, and pair hopping J', with the details given in Appendix B, and apply the Kanamori relations $U = U' + 2J$ and $J = J'$ to reduce the number of independent parameters. These bare interactions provide the initial values of the running interaction vertices (versus a decreasing energy scale) in SM-FRG. A general interaction vertex function can be decomposed as

$$V^{\alpha,\beta;\gamma,\delta}_{\mathbf{k},\mathbf{k}',\mathbf{q}} \to \sum_m S_m(\mathbf{q})\phi^{\alpha,\beta}_m(\mathbf{k},\mathbf{q})\left[\phi^{\gamma,\delta}_m(\mathbf{k}',\mathbf{q})\right]^*, \qquad (1)$$

either in the particle-particle (p-p) or particle-hole (p-h) channel. Here, $(\alpha,\beta,\gamma,\delta)$ are dummy labels for orbital and spin indices, $\mathbf{q}$ is the collective momentum, and $\mathbf{k}$ (or $\mathbf{k}'$) is an internal momentum of the Fermion bilinears $\psi^\dagger_{\mathbf{k}+\mathbf{q},\alpha}\psi^\dagger_{-\mathbf{k},\beta}$ and $\psi^\dagger_{\mathbf{k}+\mathbf{q},\alpha}\psi_{\mathbf{k},\beta}$ in the p-p and p-h channels, respectively. The fastest growing eigenvalue $S(\mathbf{Q})$ implies an emerging order associated with a collective wave vector $\mathbf{Q}$ and eigenfunction (or form factor) $\phi(\mathbf{k},\mathbf{Q})$. The divergence scale provides an upper limit of the ordering temperature. In the spin-invariant case one can further resolve spin-density-wave (SDW) and charge-density-wave (CDW) in the p-h channel. In the p-p channel $\mathbf{Q} = 0$ is always realized at low energy scale due to the Cooper mechanism. More technical details can be found in the Appendix A and elsewhere [23,24].

III. RESULTS AND DISCUSSION

A. Five-orbital model without SOC

We first consider the case in the absence of SOC, where the system is SU(2) invariant. The FRG flow versus the running energy scale Λ (the infrared cutoff of the Matsubara frequency) for $U = 3$ eV and $J = U/4$ is shown in Fig. 2(a). Since the

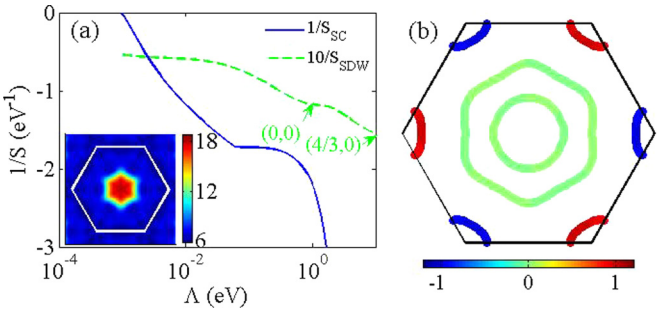

FIG. 2. (Color online) Results for the five-orbital model without SOC. (a) FRG flow of $1/S_{\mathrm{SC,SDW}}$ versus Λ. (All interactions are in units of eV.) The arrows indicate snapshots of the leading $\mathbf{q}/\pi$ for S_{SDW} during the flow. The inset shows $|S_{\mathrm{SDW}}(\mathbf{q})|$ in the momentum space at the final energy scale. The white hexagonal is the Brillouin zone. (b) The gap function $\Delta(\mathbf{k})$ on the Fermi surfaces.

CDW channel remains weak at low energy scales, we shall not address it henceforth. The interaction in the SDW channel, $S_{\rm SDW}$, is enhanced in the intermediate stage and levels off at low-energy scales. The associated collective momentum $\mathbf{Q}$ evolves from $\mathbf{Q} = (4/3,0)\pi$ (and its symmetry images) due to high-energy particle-hole excitations between states around Γ and K. It however settles down at $\mathbf{Q} = 0$. The inset of Fig. 2(a) shows $S_{\rm SDW}(\mathbf{q})$ versus $\mathbf{q}$ at the final stage of the flow. A broad peak around $\mathbf{q} = 0$ is apparent. The form factor $\phi_{\rm SDW}$ turns out to be dominated by site-wise spins from the (d_{xz},d_{yz}) orbitals, in accordance with the VHS near the Fermi level in the α band. The strong ferromagnetic fluctuations here are also consistent with the magnetic solutions by LDA [19]. Attractive pairing interactions, $S_{\rm SC}$ (for $\mathbf{Q} = 0$), are enhanced significantly as $S_{\rm SDW}$ grows (in magnitude). The cusp in the evolution of $S_{\rm SC}$ is a level crossing of (or change of pairing symmetry in) the leading pairing function $\phi_{\rm SC}(\mathbf{k})$. Eventually $S_{\rm SC}$ diverges so the system will develop SC below the divergence energy scale. To describe the momentum dependence in the (matrix) function $\phi_{\rm SC}(\mathbf{k})$, we introduce the following lattice harmonics

$$c_n = \cos(\mathbf{k}\cdot\mathbf{b}_n), \quad s_n = \sin(\mathbf{k}\cdot\mathbf{b}_n), \tag{2}$$

where $\mathbf{b}_{n=1,2,3}$ are the principle translation vectors $(1,0)$, $(-1/2,\sqrt{3}/2)$ and $(-1/2,-\sqrt{3}/2)$, respectively. Up to a global scale, we find

$$\phi_{SC}(\mathbf{k}) \sim (0.68 - 0.04\sum_n c_n)i\tau_2 - 0.14i\sum_n s_n\tau_0, \tag{3}$$

where the Pauli τ-matrices operate on (d_{xz},d_{yz}) orbitals. The other elements, including those from the other orbitals, are about two orders of magnitude smaller than the leading one. The gap function is clearly odd in orbital-momentum space, with f-wave symmetry [35], thus the spin part must be a triplet by fermion antisymmetry (with three-fold degeneracy because of spin invariance). We can project the gap function in the (spin-degenerate) band basis as $\Delta_{\mathbf{k}} = \langle\mathbf{k}|\phi_{\rm SC}|\mathbf{k}\rangle$ where $|\mathbf{k}\rangle$ is a Bloch state. As shown in Fig. 2(b), $\Delta(\mathbf{k})$ is mainly on the α pocket and has an f-wave symmetry in agreement with the above analysis. The maximum amplitudes of $|\Delta(\mathbf{k})|$ on the γ_1 and γ_2 pockets are about 400 times smaller than on the α pockets. We conclude that the α band is active, while the γ_1 and γ_2 bands are passive for SC. This is an interesting analog to the situation in Sr_2RuO_4, [27] except that TRS is respected here.

B. Effective two-orbital model with SOC

It is possible to switch on SOC at this stage. However, if all orbitals and form factors are to be kept the numerical demand is beyond our limit. (The computational complexity is discussed in Appendix A). Instead, we shall consider an effective two-orbital model with the (d_{xz},d_{yz}) orbitals and SOC, guided by the above observation that the α band is predominantly active. The validity of such a two-orbital model is justified in Appendix B.

The atomic SOC can be written as $H_{\rm SOC} = -\frac{\lambda}{2}\sum_i \psi_i^\dagger\tau_2\sigma_3\psi_i$. Here, the Pauli matrix σ acts on spins. A fit to a relativistic band-structure calculation [19] yields $\lambda \sim 0.24$ eV. The spin-split band structure is shown in Fig. 1(c), and the corresponding FS is shown in Fig. 1(d) for $\mu = 9.85$ eV.

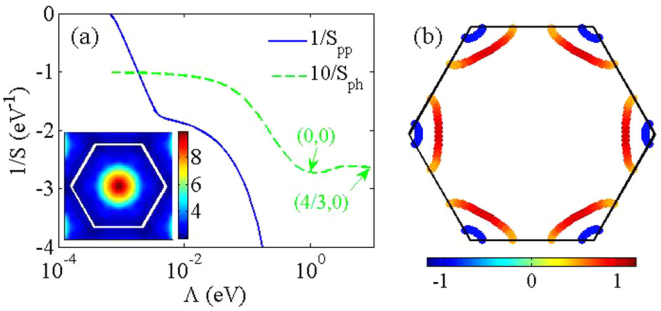

FIG. 3. (Color online) The results for a two-orbital model with SOC. (a) FRG flow of $1/S_{pp,ph}$ versus Λ. The arrows indicate snapshots of the leading $\mathbf{q}/\pi$ for S_{ph} during the flow. The inset shows $|S_{ph}(\mathbf{q})|$ in the momentum space at the final energy scale. The white hexagonal is the Brillouin zone. (b) The gap function $\Delta(\mathbf{k})$ on the Fermi surfaces.

In the presence of SOC, we apply the SM-FRG extended for spin-resolved fully antisymmetrized interactions [24]. The FRG flow for $U = 3$ eV and $J = U/4$ is shown in Fig. 3(a). The interaction in the p-h channel, S_{ph}, behaves qualitatively similar to $S_{\rm SDW}$ in Fig. 2(a). The inset shows $S_{ph}(\mathbf{q})$ versus $\mathbf{q}$ at the final stage of the flow. There is a rounded hump at the zone center, but it is otherwise similar to the inset of Fig. 2(a). The form factor with the dominant momentum $\mathbf{Q} = 0$ is given by, with twofold degeneracy, $\phi_{ph}(\mathbf{k},\mathbf{Q}) \sim 0.35\tau_0(\sigma_x \pm i\sigma_y)$. (Without SOC the form factor would be threefold degenerate.) These form factors are clearly spinlike and are aligned in the plane. The $\mathbf{k}$ independence in the leading term means the spin is predominantly site-local. Thus ferromagnetic spin fluctuations with *easy-plane anisotropy* survive against SOC, although the global magnitude is weakened by roughly a factor of two as compared to the case in the absence of SOC. Because of the surviving ferromagnetic spin fluctuations, attractive pairing interaction S_{pp} is also induced and eventually diverges. To reveal the spin and orbital contents explicitly, we now write the matrix pairing form factor as $\phi_{pp}(\mathbf{k}) = (g_{\mathbf{k}} + \gamma_{\mathbf{k}})i\sigma_2$ with singlet and triplet parts $g_{\mathbf{k}}$ and $\gamma_{\mathbf{k}}$, respectively. For the case in Fig. 3, we find

$$g_{\mathbf{k}} \sim -\left(0.06 + 0.04\sum_n c_n\right)\tau_0 - 0.1\sum_n s_n\tau_2 + 0.09[(c_3 - c_2)\tau_1 + (2c_1 - c_2 - c_3)\tau_3/\sqrt{3}], \tag{4}$$

$$\gamma_{\mathbf{k}} \sim -0.34\sum_n s_n\tau_0\sigma_3 + \left(0.03 - 0.17\sum_n c_n\right)\tau_2\sigma_3. \tag{5}$$

A few remarks are in order. First, the singlet part $g_{\mathbf{k}}$ transforms as s wave [35], but the amplitude is relatively small. The dominant part is the $\tau_{0,2}\sigma_3$ terms in γ_k describing f-wave triplet pairing. The fact that these terms are triplets is because the τ_0 term (τ_2 term) is odd in $\mathbf{k}$ (in the orbital space). The triplet pairing is clearly triggered by ferromagnetic fluctuations. The singlet and triplet components mix due to the lack of local inversion symmetry as well as SOC, and we observe that they transform identically upon *joint spin-lattice rotations*. One can

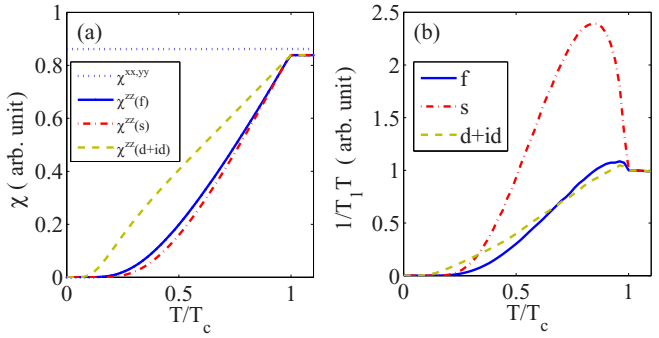

FIG. 4. (Color online) (a) Spin susceptibility $\chi^{xx,yy}$(blue dotted line) and χ^{zz}(blue solid line) versus temperature for the f wave derived from SMFRG, and χ^{zz} for s wave (red dash-dotted line) and chiral $d_{x^2-y^2}+id_{xy}$−wave (green dashed line). The change in $\chi^{xx,yy}$ versus temperature and gap function is almost invisible for the SOC scale $\lambda = 0.24$ eV. (b) The spin lattice relaxation rate $1/T_1T$ versus temperature for the f wave derived from SMFRG (blue solid line), and for s wave (red dash-dotted line) and chiral $d_{x^2-y^2}+id_{xy}$ wave (green dashed line), with Dynes factor $\eta = 0.01T_c$.

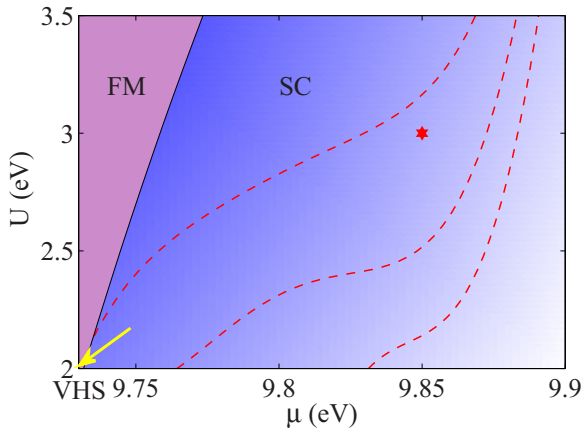

FIG. 5. (Color online) A schematic phase diagram in (U,μ) space with $J = U/4$. The hexagram indicates the case discussed in the text, and the dashed lines indicate equal-value contours for the SC critical scale Λ_c, which changes from 0.01 meV to 0.1 meV to 1 meV from right to left. The ferromagnetic order sets in near the VHS (highlighted by the arrow).

dub such a pairing as s^* wave according to Ref. [28]. Second, TRS is respected in the above pairing function. Thus we can project it in the band basis as follows:

$$\Delta_{\mathbf{k}} = \langle \mathbf{k}|\phi_{pp}(\mathbf{k})(|-\mathbf{k}\rangle)^* = \langle \mathbf{k}|g_{\mathbf{k}} + \gamma_{\mathbf{k}}|\mathbf{k}\rangle, \qquad (6)$$

where $|\mathbf{k}\rangle$ is a Bloch state and $|-\mathbf{k}\rangle = i\sigma_2 K|\mathbf{k}\rangle$ is the time reversal of $|\mathbf{k}\rangle$. Since $\gamma_{\mathbf{k}}$ transforms similarly to SOC that splits the bands, it causes a sign change of $\Delta(\mathbf{k})$ across spin-split bands, as shown in Fig. 3(b) (color scale). However, the pairing gap is nodeless on each spin-split Fermi pocket. The s-wave-like sign structure versus rotations is consistent with the previous analysis in the spin-orbital basis.

We emphasize that the above $\gamma_{\mathbf{k}}$ corresponds to a triplet $\mathbf{d}$ vector along the z axis, pinned by SOC. This means the total spin of the Cooper pair along the z axis is zero, consistent with the easy-plane spin fluctuations mentioned above, and implies that in the SC state the out-of-plane spin susceptibility is suppressed, while the in-plane one can survive. This is exactly the case shown in Fig. 4(a), following from a mean field theory calculation using the pairing interaction derived from SM-FRG (see Appendix C). We also show in Fig. 4(a) the spin susceptibilities if the gap function is given by a fully gapped singlet s wave (red dash-dotted line) and the chiral $d_{x^2-y^2}+id_{xy}$ wave (green dashed line) suggested elsewhere [8,36]. We find that the change in $\chi^{xx,yy}$ versus temperature is almost invisible because of the large SOC scale $\lambda = 0.24$ eV [37]. On the other hand, χ^{zz} drops exponentially right below half of T_c for our f-wave and the s-wave gaps. In contrast, it is quasilinear down to $T_c/4$ for the chiral $d_{x^2-y^2}+id_{xy}$ wave gap (which is small on the inner α pocket, and in fact vanishes at the K and K' points). In Ref. [21], the Knight shift result is well fitted by an s-wave gap, but it may also be well fitted by the f-wave gap according to the above results. Figure 4(b) shows the nuclear spin-lattice relaxation rate $1/T_1T$ versus temperature using the pairing function derived from SMFRG (blue solid line), or given by the s-wave (red dash-dotted line) and chiral $d_{x^2-y^2}+id_{xy}$-wave (green dashed line) gap. (See Appendix C for technical details.) In the calculation we used a Dynes factor $\eta = 0.01T_c$ to account for quasiparticle relaxation. We find that $1/T_1T$ has a small peak below T_c for our f-wave pairing, while there is a strong peak for the s-wave pairing. The peak is minute for chiral $d_{x^2-y^2}+id_{xy}$-wave pairing. Experimentally, a Hebel-Slichter peak is found in Ref. [21] but is barely visible in Ref. [22].

We have performed systematic calculations by varying the bare interaction parameters and the doping level (or the Fermi level). The results are summarized as a schematic phase diagram in Fig. 5. The pairing scale Λ_c increases with hole doping (or decreasing Fermi energy), until the ferromagnetic phase is approached in the immediate vicinity of the VHS, and in a large regime $\Lambda_c \sim 0.1-1$ meV, of the same order of the experimental T_c. We have chosen a fixed ratio $J/U = 1/4$ here, but the results are qualitatively robust down to $J/U = 1/12$. However, if we set $U = U'$ and $J = 0$ (up to a small J'), we find d-wave pairing as in Ref. [36]. (A direct comparison to our results is not applicable since the "local" interaction in Ref. [36], defined in the band basis, is not necessarily local in the orbital basis due to orbital hybridizations. Moreover, this interaction is assumed to bear a pseudo-spin symmetry that is apparently absent in the more fundamental local interactions defined in the orbital basis.)

Finally we discuss the influence of interlayer coupling. The interplane pairing turns out to be negligible, and the only effect in the double-layer model is that the singlet component $g_{\mathbf{k}}$ changes sign from one layer to the other. Therefore the global symmetry of the gap function becomes the A_{2u} representation of the D_{3d} group, consistent with the symmetry analysis in Ref. [8]. In addition, we find the spin correlation is ferromagnetic within the plane, but is antiferromagnetic across the plane, in agreement with the LDA calculation [19].

IV. SUMMARY

We investigated the pairing mechanism in the SrPtAs superconductor. We find that out of the five d orbitals, the $d_{xz,yz}$ orbitals are active for superconductivity, and the triplet

pairing is driven by FM-like spin fluctuations in SrPtAs. We remark that the pairing function given here respects TRS in the bulk. However, TRSB at grain boundaries is possible and was actually argued as one of the possibilities in the μSR experiment [20]. Another possibility is that the strong ferromagnetic fluctuations at low energies behave as instantaneous magnetic moments to fast probes and can also cause muon spin relaxations. Finally, we did not consider the electron-phonon coupling, given the unconventional pairing revealed in the μSR experiment. While we can not rule out the role of electron-phonon coupling in driving the superconductivity, our results do provide a clear picture as to what correlation would lead to if it were the main driving force.

ACKNOWLEDGMENTS

We thank M. Sigrist for communications, and C. Platt, W. Hanke, and R. Thomale for communications and previous collaborations. The project was supported by NSFC (under Grant No. 10974086 and No. 11023002) and the Ministry of Science and Technology of China (under Grant Nos. 2011CBA00108 and 2011CB922101). The numerical calculations were performed in the High Performance Computing Center of Nanjing University.

APPENDIX A: THE SM-FRG METHOD

The technical details of SM-FRG have appeared in parts (for cases with or without SOC) in Refs. [4], [23], and [24] and will be rewritten here for self-completeness. The idea of FRG [29] is to perform continuous perturbation theory in terms of the change of the phase space. Starting from a high energy window, one obtains the one-particle-irreducible (1PI) vertex functions and asks how they change if the infrared limit of the energy window is lowered infinitesimally. This process is repeated versus a running energy scale, i.e., the infrared cutoff Λ, resulting in a flow of the 1PI vertex functions. The Λ-dependent vertex functions provide an effective description of the system at the energy scale Λ. A diverging four-point vertex function implies an instability of the normal state toward an emerging order, and the critical scale Λ_c is an estimate of the upper limit of the ordering temperature.

Consider a generic four-point vertex function Γ in the interaction $\psi^\dagger_{\mathbf{k}_1}\psi^\dagger_{\mathbf{k}_2}(-\Gamma^{1234}_{\mathbf{k}_1,\mathbf{k}_2,\mathbf{k}_3,\mathbf{k}_4})\psi_{\mathbf{k}_3}\psi_{\mathbf{k}_4}$. The minus sign before Γ is a convention for later convenience. The labels 1, 2, 3, and 4 represent orbital-spin indices, and the momentum conservation requires $\mathbf{k}_1+\mathbf{k}_2=\mathbf{k}_3+\mathbf{k}_4$. Figures 6(a)–6(c) are rearrangements of Γ in the pairing (P), crossing (C), and direct (D) channels, each with a collective momentum $\mathbf{q}$. The dependence on the other two momenta can be decomposed as

$$\begin{aligned}\Gamma^{1234}_{\mathbf{k}+\mathbf{q},-\mathbf{k},-\mathbf{p},\mathbf{p}+\mathbf{q}} &\to \sum_{mn} f_m(\mathbf{k},1,2)P_{mn}(\mathbf{q})f^*_n(\mathbf{p},4,3),\\ \Gamma^{1234}_{\mathbf{k}+\mathbf{q},\mathbf{p},\mathbf{k},\mathbf{p}+\mathbf{q}} &\to \sum_{mn} f_m(\mathbf{k},1,3)C_{mn}(\mathbf{q})f^*_n(\mathbf{p},4,2),\\ \Gamma^{1234}_{\mathbf{k}+\mathbf{q},\mathbf{p},\mathbf{p}+\mathbf{q},\mathbf{k}} &\to \sum_{mn} f_m(\mathbf{k},1,4)D_{mn}(\mathbf{q})f^*_n(\mathbf{p},3,2).\end{aligned} \tag{A1}$$

Here $\{f_m\}$ is a set of orthonormal basis functions of the internal momentum $\mathbf{k}$ (or $\mathbf{p}$) and a pair of orbital-spin labels. For brevity we shall suppress the orbital-spin labels in f_m unless indicated otherwise. The momentum dependence in f_m is given by

$$f_m(\mathbf{k})=\sum_{\mathbf{r}} f_m(\mathbf{r})\exp(-i\mathbf{k}\cdot\mathbf{r}), \tag{A2}$$

where $f_m(\mathbf{r})$ may be chosen to transform according to an irreducible representation of the underlying point group G (which is C_{3v} in the main text), and $\mathbf{r}$ is a bond vector connecting the fermion bilinear, e.g., the two ψ's (or two $\psi^\dagger$'s) in Fig. 6(a), or one ψ and one $\psi^\dagger$ in Figs. 6(b) and 6(c). We notice the decoupling in each channel respects momentum conservation exactly, since three and only three independent momenta are accessed. On the other hand, if the basis functions form a complete set in momentum, spin and orbital spaces, the above decomposition is exact in each channel, and P, C, and D are simply different aliases of Γ.

In the absence of SOC, spin conservation enables us to set the spin labels $\mu=\lambda$ and $\nu=\sigma$ in Fig. 6, and in fact they can be suppressed completely. Under this convention, the one-loop contributions to the flow of the 1PI vertex functions are shown in Fig. 7, where (a) and (b) are flows in the pairing and crossing channel, and (c)–(e) in the direct channel. We denote such contributions as, in matrix form,

$$\begin{aligned}\partial P/\partial\Lambda &= P\chi'_{pp}P, \quad \partial C/\partial\Lambda = C\chi'_{ph}C,\\ \partial D/\partial\Lambda &= (C-D)\chi'_{ph}D + D\chi'_{ph}(C-D),\end{aligned} \tag{A3}$$

where the collective momentum $\mathbf{q}$ is left implicit for brevity, and

$$\begin{aligned}(\chi'_{pp})_{mn} &= \frac{\partial}{\partial\Lambda}\int\frac{d\omega_n}{2\pi}\int\frac{d^2\mathbf{p}}{S_{\mathrm{BZ}}}f^*_m(\mathbf{p})G(\mathbf{p}+\mathbf{q},i\omega_n)\\ &\quad\times G(-\mathbf{p},-i\omega_n)f_n(\mathbf{p})\theta(|\omega_n|-\Lambda)\\ &= -\frac{1}{2\pi}\int\frac{d^2\mathbf{p}}{S_{\mathrm{BZ}}}f^*_m(\mathbf{p})G(\mathbf{p}+\mathbf{q},i\Lambda)\\ &\quad\times G(-\mathbf{p},-i\Lambda)f^*_n(\mathbf{p}) \ +(\Lambda\to-\Lambda),\\ (\chi'_{ph})_{mn} &= \frac{\partial}{\partial\Lambda}\int\frac{d\omega_n}{2\pi}\int\frac{d^2\mathbf{p}}{S_{\mathrm{BZ}}}f^*_m(\mathbf{p})G(\mathbf{p}+\mathbf{q},i\omega_n)\\ &\quad\times G(\mathbf{p},i\omega_n)f_n(\mathbf{p})\theta(|\omega_n|-\Lambda)\\ &= -\frac{1}{2\pi}\int\frac{d^2\mathbf{p}}{S_{\mathrm{BZ}}}f^*_m(\mathbf{p})G(\mathbf{p}+\mathbf{q},i\Lambda)\\ &\quad\times G(\mathbf{p},i\Lambda)f_n(\mathbf{p}) \ +(\Lambda\to-\Lambda),\end{aligned} \tag{A4}$$

where G is the free fermion Green's function, and S_{BZ} is the total area of the Brillouin zone. Here $\Lambda>0$ is the infrared cutoff of the Matsubara frequency $|\omega_n|$. As in usual

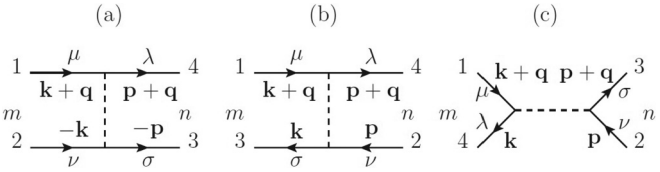

FIG. 6. A generic four-point vertex Γ^{1234} is rearranged into P, C, and D channels in (a)–(c), respectively. Here $\mathbf{k},\mathbf{q},\mathbf{p}$ are momenta, μ,ν,σ,λ are spin indices, and m,n denote the basis functions.

FRG implementation, the self-energy correction and frequency dependence of the vertex function are ignored.

We observe that ∂P, ∂C, and ∂D contribute independently to the full change $d\Gamma$, which should be reinterpreted as dP, dC, and dD in the respective channels. This can be formally written as

$$dK/d\Lambda = \partial K/\partial\Lambda + \sum_{K'\neq K} \hat{\mathcal{P}}_{KK'}[\partial K'/\partial\Lambda], \tag{A5}$$

for $K = P$, C, and D. Here $\hat{\mathcal{P}}_{KK'}$ is a projection operator via Eqs. (A1): It brings the vertex in the K' channel into the form of the generic Γ, which is subsequently decomposed into the K channel. In Eq. (A5) the projected terms are overlaps among the three different channels. It is those terms that allow pairing to be induced by virtual particle-hole scattering processes. We remark that without the mutual overlap, the flow would correspond to ladder approximations in separate channels. By taking care of the channel overlap, the full flow in each channel is a faithful representation of the flow of Γ if the decomposition in each line of Eq. (A1) is exact. Clearly FRG treats all channels on equal footing, and the reliability goes far beyond the scope of simple ladder approximation that overestimates a particular channel while ignoring the others.

At each energy scale Λ, the effective interaction in the superconducting (SC), spin-density wave (SDW), and charge-density wave (CDW) channels are given by $V_{\rm SC} = -P$, $V_{\rm SDW} = C$, and $V_{\rm CDW} = C - 2D$, respectively. To see the leading instability, we perform singular-value decomposition at each collective momentum $\mathbf{q}$, for $V = V_{\rm SC/SDW/CDW}$,

$$V_{mn}(\mathbf{q}) \to \sum_i S_i(\mathbf{q})\xi_i(m)\eta_i(n), \tag{A6}$$

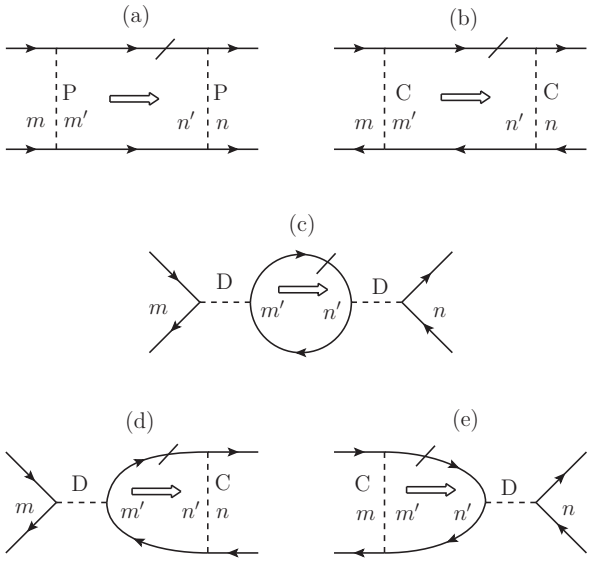

FIG. 7. One loop diagrams contributing to the flow of the the four-point vertex function in the pairing channel (a), crossing channel (b), and direct channel (c)–(e). Here $m,m'n,n'$ denote basis functions, while the momentum and orbital indices are left implicit. The open arrows indicate the flow of the collective momentum. The slashed lines are single-scale fermion propagators. The slash can be placed on either internal line associated with the loop.

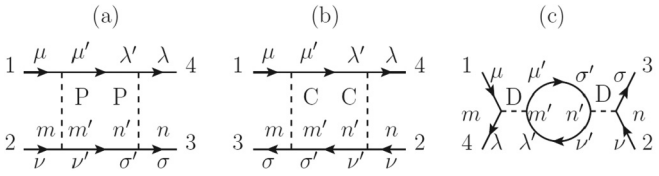

FIG. 8. One loop diagrams contributing to the flow of the the fully antisymmetrized four-point vertex function in the pairing channel (a), crossing channel (b), and direct channel (c), respectively. Here $m,m'n,n'$ denote form factors, and μ,ν,σ,λ denote spin and orbital indices.

where $S_i(\mathbf{q})$ is the singular value of the ith singular mode, and ξ_i and η_i are the right and left eigenvectors of $V(\mathbf{q})$, respectively. We fix the phase of the eigenvectors by requiring $\mathrm{Re}[\sum_m \xi_i(m)\eta_i(m)] > 0$ so that $S_i < 0$ corresponds to an attractive mode. In the pairing channel $\mathbf{q} = \mathbf{Q}_{SC} = 0$ addresses the Cooper instability. In the SDW/CDW channel, the potential ordering wave vector $\mathbf{q} = \mathbf{Q}$ is chosen where $S(\mathbf{q})$ is maximally attractive. An eigenmode is associated with a form factor via Eq. (A1),

$$\phi_i^{\alpha,\beta}(\mathbf{k}) = \sum_m \xi_i(m) f_m(\mathbf{k},\alpha,\beta). \tag{A7}$$

Here we make it explicit that (α,β) is a pair of orbital labels associated with the fermion bilinear in the respective channel. In terms of such form factors, we can rewrite the interaction vertex as, for a given $\mathbf{q}$,

$$V^{\alpha,\beta;\gamma,\delta}_{\mathbf{k},\mathbf{k}',\mathbf{q}} = \sum_i S_i(\mathbf{q})\phi_i^{\alpha,\beta}(\mathbf{k})\left[\phi_i^{\gamma,\delta}(\mathbf{k}')\right]^*. \tag{A8}$$

The real-space counterpart of the form factor,

$$\phi_i^{\alpha,\beta}(\mathbf{r}) = \sum_m \xi_i(m) f_m^{\alpha,\beta}(\mathbf{r}), \tag{A9}$$

determines the real-space structure of a candidate order parameter. For example, in the SC channel the most attractive mode $\phi_{\rm SC}(\mathbf{r})$ describes pairing on bond $\mathbf{r}$, and in the SDW/CDW channel $\phi_{\rm SDW/CDW}(\mathbf{r})$ describes spin/charge order on bond $\mathbf{r}$. Thus both site-local ($\mathbf{r} = 0$) and bond-centered ($\mathbf{r} \neq 0$) order parameters (and their combinations) in any channel can be captured. Notice that since ξ evolves during the FRG flow, so does ϕ. The FRG automatically determines the most attractive mode with the best form factor. *We call such an FRG scheme the singular-mode FRG (SM-FRG).*

In the presence of SOC, the spins are not conserved during fermion propagation, and we need to associate a pair of spin indices in f_m. We also need to antisymmetrize the vertex functions explicitly so that the running vertices satisfy fermion antisymmetry. In this case, the matrices C and D are not independent, since $D = -C$. In the following, D is used for bookkeeping purposes. Figures 8(a)–8(c) show the one-loop contributions to the flow of the 1PI vertex functions, with

$$\begin{aligned} \partial P/\partial\Lambda &= P\chi'_{pp}P/2, \\ \partial C/\partial\Lambda &= C\chi'_{ph}C, \\ \partial D/\partial\Lambda &= -D\chi'_{ph}D, \end{aligned} \tag{A10}$$

where χ'_{pp} and χ'_{ph} are formally identical to that in Eq. (A4). As in the spin-conserved case, the full flow equations are given by Eq. (A5). We notice that the theory reduces to the previous case if spin invariance is assumed in the starting Hamiltonian.

The effective interaction in the particle-particle (pp) and particle-hole (ph) channels are given by $V_{pp} = -P/2$ and $V_{ph} = C$, respectively. By singular-value decomposition as in Eq. (A6) we determine the leading instability in the pp and ph channels. The (matrix) form factor $\phi^{\alpha,\beta}(\mathbf{k})$ can be constructed for leading eigenmodes as in Eq. (A7), except that here α and β include spin labels also.

A few remarks are in order. First, an emerging collective mode is always associated with a short-range order parameter. For example, the conventional s-wave pairing in the BCS model is local in real space (since the pairing function is independent of momentum), the conventional spin ordered phase is associated with site-local spins. In cuprates, the d-wave pairing occurs primarily on nearest-neighbor bonds, and the $s_{\pm}$-wave pairing in iron pnictides occurs on bonds up to the second neighbors. These examples show that in practice it is sufficient to limit $\mathbf{r}$ in the basis function $f_m(\mathbf{r})$ within a given range in order to capture the leading ordering tendencies. We emphasize that the truncation for $\mathbf{r}$ does not limit the collective momentum $\mathbf{q}$ (or equivalently the setback distance between two fermion bilinears). This is important for us to address the thermodynamic limit. In our calculations we choose $\mathbf{r}$ up to the second neighbors, and we checked that longer bonds do not change the results qualitatively (and even quantitatively). Second, the number of basis functions f_m is $N = N_{\mathbf{r}} N_o^2 N_s^2$ where $N_{\mathbf{r}}$ is the number of $\mathbf{r}$'s used for $f_m(\mathbf{r})$, and $N_{o/s}$ is the number of orbitals/spins. In the spin-invariant system the spin label does not enter the flow equations explicitly, so effectively $N_s = 1$, while in the presence of SOC we take full account of spins, so that $N_s = 2$. In any case the computational complexity in the loop integrations scales as N^4, and hence scales as $N_o^8 N_s^8$. The quick increase of the complexity versus the number of orbitals is the main computational difficulty in the SM-FRG. Finally, we remark that our SM-FRG works in the orbital-spin basis. So all relevant bands are taken into account. But the result can be easily transformed into the band basis by simple unitary transformations.

APPENDIX B: RANDOM PHASE APPROXIMATION FOR THE FIVE-ORBITAL MODEL WITH SOC

As discussed in the above, the computational complexity of the SM-FRG scales as $N_{\mathbf{r}}^4 N_o^8 N_s^8$. This forbids us from including all of the five orbitals while retaining all lattice form factors up to the second neighbor bonds (so that $N_{\mathbf{r}} = 13$). In order to judge the relative importance of the five orbitals in the presence of SOC, we compromise to keep the onsite form factor only (so that $N_{\mathbf{r}} = 1$), and ignore the overlaps between the pp and ph channels. This enables analytical solution to the flow equations, and the result is identical to that from the standard ladder approximation in the respective channels, except for the infrared energy cutoff. In the ph channel, it is usually referred to as the random phase approximation (RPA). We should remark that in the present setting, there is no divergence in P for repulsive bare interactions, but divergence in C (or in the ph channel) is likely for the RPA scheme overestimates favorable instabilities. We avoid such a divergence by choosing a suitably low energy scale Λ, at which we transform $-P_\Lambda/2$ and $C_\Lambda - C_\infty$ into the band basis. (The subtraction of the initial value C_∞ is necessary to remove double counting. The subscript Λ will be henceforth suppressed for brevity.) We rewrite all of them in the form of pair scattering. They contribute independently to $V_{\mathrm{SC}}(\mathbf{k},n;\mathbf{k}',n')$, the pairing interaction for a $(\mathbf{k}', -\mathbf{k}')$ electron pair on the n' band to be scattered into a $(\mathbf{k}, -\mathbf{k})$ pair on the n band. The collection of contributions here can be understood as accounting for the channel overlaps once and forever. The pairing interaction is then substituted into the linearized Eliashberg equation

$$-\sum_{n'} \int \frac{d^2\mathbf{k}'}{S_{BZ}} V_{SC}(\mathbf{k},n;\mathbf{k}',n') T \sum_{\omega_n} \times G_{n'}(\mathbf{k}',i\omega_n) G_{n'}(-\mathbf{k}', -i\omega_n) \phi_{n'}(\mathbf{k}') = \lambda \phi_n(\mathbf{k}) \quad \text{(B1)}$$

to get the leading eigenmode of Cooper pairing with the largest eigenvalue λ. Here $T \sim \Lambda$ is the temperature, $G_n(\mathbf{k},i\omega_n)$ is the Green's function in the n band, and ω_n is the Matsubara frequency. The procedure described here is equivalent to that in the conventional RPA scheme [38,39].

To proceed, we need to specify the atomic SOC involving all of the five d orbitals, $H_{\mathrm{SOC}} = -\lambda/2 \sum_i \psi_i^\dagger \mathbf{L} \cdot \sigma \psi_i$. Here, σ are Pauli matrices. $\mathbf{L} = (L_x, L_y, L_z)$ is the angular momentum, with the following *nonzero* matrix elements in the basis $\psi^t = (d_{3z^2-r^2}, d_{xz}, d_{yz}, d_{x^2-y^2}, d_{xy})$,

$$\begin{aligned} L_x^{25} &= -L_x^{52} = -L_x^{34} = L_x^{43} = i; \\ L_x^{13} &= -L_x^{31} = \sqrt{3}i; \\ L_y^{35} &= -L_y^{53} = L_y^{24} = -L_y^{42} = -i; \\ L_y^{12} &= -L_y^{21} = -\sqrt{3}i; \\ L_z^{23} &= -L_z^{32} = -i; \\ L_z^{45} &= -L_z^{54} = -2i. \end{aligned} \quad \text{(B2)}$$

A fit to a relativistic band-structure calculation yields $\lambda \sim 0.24$ eV. On the other hand, the local interaction Hamiltonian is given by

$$\begin{aligned} H_I = {} & U \sum_{i\alpha} n_{i\alpha\uparrow} n_{i\alpha\downarrow} + U' \sum_{i,\alpha>\beta} n_{i,\alpha} n_{i,\beta} \\ & + J \sum_{i,\alpha>\beta,\sigma\sigma'} c^\dagger_{i\alpha\sigma} c_{i\beta\sigma} c^\dagger_{i\beta\sigma'} c_{i\alpha\sigma'} \\ & + J' \sum_{i,\alpha\neq\beta} c^\dagger_{i\alpha\uparrow} c^\dagger_{i\alpha\downarrow} c_{i\beta\downarrow} c_{i\beta\uparrow} \end{aligned} \quad \text{(B3)}$$

with intraorbital repulsion U, interorbital repulsion U', Hund's rule spin exchange J, and pair hopping term J'. We apply the Kanamori relations $U = U' + 2J$ and $J = J'$ to reduce the number of independent parameters. We set $U = 1$ eV and $J = U/4$ here for illustration.

Figure 9(a) shows the leading eigenvalue of the RPA-enhanced ph-channel susceptibility $\chi(\mathbf{q})$ (a matrix in the spin-orbital basis). It is peaked around the zone center, consistent with the strong ferromagnetic spin fluctuations found in the effective two-orbital model in Sec. III B. Figure 9(b)

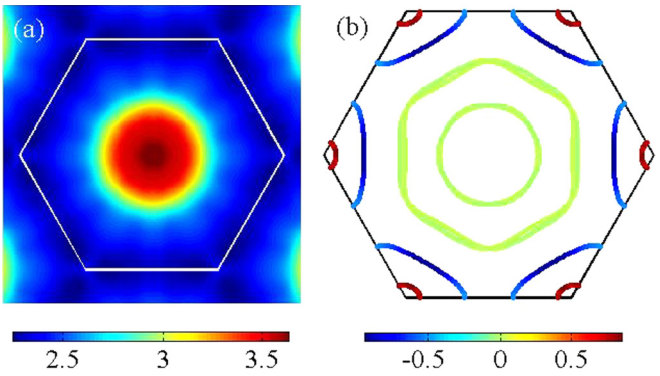

FIG. 9. (Color online) The RPA results for $U = 1$ eV, $J = U/4$. (a) The leading eigenvalue of the matrix susceptibility $\chi(\mathbf{q})$ as a function of $\mathbf{q}$ in the Brillouin zone. (b) The leading gap function on the Fermi surfaces.

shows the gap function on the Fermi surfaces for the leading attractive eigenmode of $V_{\rm SC}(\mathbf{k},n;\mathbf{k}',n')$, obtained along the line described above. The gap function on the α pockets around K and K' is closely similar to that in the effective two-orbital model in Sec. III B. Moreover, the pairing amplitude on the $\gamma_{1,2}$ pockets is about $1/40$ of that on the α pockets. This ratio is larger than that for the five-orbital model without SOC in Sec. III A, apparently arising from the interband proximity effect caused by the SOC. Yet the ratio is still small enough for us to identify the α pockets as the active bands. Since the latter are dominated by the $d_{xz/yz}$ orbitals, the effective two-orbital model in Sec. III B serves as a useful minimal model.

APPENDIX C: MEAN FIELD CALCULATIONS IN THE SUPERCONDUCTING PHASE

If the pp channel is leading, the effective low-energy Hamiltonian is given by

$$H = H_0 + \frac{V_{\rm eff}}{N}\sum_{\mathbf{k},\mathbf{k}'} B^\dagger_{\mathbf{k}} B_{\mathbf{k}'} \tag{C1}$$

where $V_{\rm eff} < 0$ is the pairing interaction, N is the number of lattice sites, and $B^\dagger_{\mathbf{k}}$ is the pairing operator

$$B^\dagger_{\mathbf{k}} = \Psi^\dagger_{\mathbf{k}}\phi_{\rm SC}(\mathbf{k})(\Psi^\dagger_{-\mathbf{k}})^T, \tag{C2}$$

with the form factor $\phi_{\rm SC}(\mathbf{k})$ determined by SM-FRG. Here $\Psi^\dagger$ is a spinor creation field for all orbital/spin degrees of freedom. The mean-field Hamiltonian can be written as

$$H_{\rm MF} = H_0 + \sum_{\mathbf{k}}(\Delta B^\dagger_{\mathbf{k}} + \text{H.c.}), \tag{C3}$$

subject to the self-consistent condition

$$\Delta = \frac{V_{\rm eff}}{N}\sum_{\mathbf{k}}\langle B_{\mathbf{k}}\rangle. \tag{C4}$$

In the calculation, we choose $V_{\rm eff}$ so that the mean field T_c is close to the FRG divergence scale.

The uniform spin susceptibility $\chi^{\alpha\alpha} = \chi^{\alpha\alpha}(\mathbf{q}\to 0)$ is given by

$$\chi^{\alpha\alpha}(\mathbf{q}) = -\frac{T}{N}\sum_{\mathbf{k},\omega_n}\text{Tr}[G(\mathbf{k},i\omega_n)\gamma^\alpha G(\mathbf{k}+\mathbf{q},i\omega_n)\gamma^\alpha], \tag{C5}$$

where G and γ^α are the Green's function and spin vertex (of polarity α) in the Nambu space. The trace is taken in the spin-orbital-Nambu space.

The spin-lattice relaxation rate $1/T_1T$ is associated with the low frequency dynamics of local spins and is given by

$$\begin{aligned}\frac{1}{T_1T} &= -\lim_{\nu\to 0}\sum_{\alpha\beta}\frac{g_{\alpha\beta}}{\nu}\text{ImTr}[\gamma_\alpha G_{\rm loc}(i\omega_n + i\nu_n)\\ &\quad\times\gamma_\beta G_{\rm loc}(i\omega_n)]|_{i\nu_n\to\nu+i0^+}\\ &= -\lambda^2\sum_\alpha\int d\omega\frac{\partial f}{\partial\omega}\text{Tr}[\gamma_\alpha A(\omega)\gamma_\alpha A(\omega)].\end{aligned} \tag{C6}$$

Here $g_{\alpha\beta} = \lambda^2\delta_{\alpha\beta}$ is taken as the hyperfine coupling matrix element, f is the Fermi function, and $G_{\rm loc}$ is the local Green's function, which can be expanded as

$$G_{\rm loc}(i\omega_n) = \frac{1}{N}\sum_{\mathbf{k},m}\frac{|\mathbf{k},m\rangle\langle\mathbf{k},m|}{i\omega_n - E_{\mathbf{k},m}} = \int d\omega\frac{A(\omega)}{i\omega_n-\omega}, \tag{C7}$$

where $|\mathbf{k},m\rangle$ is the eigenstate, and we defined a local spectral matrix

$$\begin{aligned}A(\omega) &= \frac{1}{N}\sum_{\mathbf{k}m}|\mathbf{k},m\rangle\langle\mathbf{k},m|\delta(\omega - E_{\mathbf{k},m})\\ &\to \frac{1}{N}\sum_{\mathbf{k}m}\frac{\eta}{\pi}\frac{|\mathbf{k},m\rangle\langle\mathbf{k},m|}{(\omega-E_{\mathbf{k},m})^2+\eta^2}.\end{aligned} \tag{C8}$$

In the last line we approximate the delta function by a Lorentzian with a Dynes factor η.

[1] Y. Nishikubo, K. Kudo, and M. Nohara, J. Phys. Soc. Jpn. **80**, 055002 (2011).
[2] P. A. Lee, N. Nagaosa, and X. G. Wen, Rev. Mod. Phys. **78**, 17 (2006).
[3] G. R. Stewart, Rev. Mod. Phys. **83**, 1589 (2011).
[4] W.-S. Wang, Z.-Z. Li, Y.-Y. Xiang, and Q.-H. Wang, Phys. Rev. B **87**, 115135 (2013).
[5] M. L. Kiesel, C. Platt, and R. Thomale, Phys. Rev. Lett. **110**, 126405 (2013).
[6] Q.-H. Wang, D.-H. Lee, and P. A. Lee, Phys. Rev. B **69**, 092504 (2004).
[7] M. L. Kiesel, C. Platt, W. Hanke, and R. Thomale, Phys. Rev. Lett. **111**, 097001 (2013).
[8] J. Goryo, M. H. Fischer, and M. Sigrist, Phys. Rev. B **86**, 100507(R) (2012).
[9] M. H. Fischer, F. Loder, and M. Sigrist, Phys. Rev. B **84**, 184533 (2011).
[10] D. Maruyama, M. Sigrist, and Y. Yanase, J. Phys. Soc. Jpn. **81**, 034702 (2012).

[11] L. P. Gor'kov and E. I. Rashba, Phys. Rev. Lett. **87**, 037004 (2001).
[12] E. Bauer, G. Hilscher, H. Michor, Ch. Paul, E. W. Scheidt, A. Gribanov, Yu. Seropegin, H. Noël, M. Sigrist, and P. Rogl, Phys. Rev. Lett. **92**, 027003 (2004).
[13] P. A. Frigeri, D. F. Agterberg, A. Koga, and M. Sigrist, Phys. Rev. Lett. **92**, 097001 (2004).
[14] P. A. Frigeri, D. F. Agterberg, and M. Sigrist, New J. Phys. **6**, 115 (2004).
[15] K. V. Samokhin, Phys. Rev. B **78**, 224520 (2008).
[16] N. Kimura, K. Ito, H. Aoki, S. Uji, and T. Terashima, Phys. Rev. Lett. **98**, 197001 (2007).
[17] H. Mukuda, T. Ohara, M. Yashima, Y. Kitaoka, R. Settai, Y. Onuki, K. M. Itoh, and E. E. Haller, Phys. Rev. Lett. **104**, 017002 (2010).
[18] I. R. Shein and A. L. Ivanovskii, Physica C **471**, 594 (2011).
[19] S. J. Youn, S. H. Rhim, D. F. Agterberg, M. Weinert, and A. J. Freeman, arXiv:1202.1604.
[20] P. K. Biswas, H. Luetkens, T. Neupert, T. Stürzer, C. Baines, G. Pascua, A. P. Schnyder, M. H. Fischer, J. Goryo, M. R. Lees, H. Maeter, F. Brückner, H.-H. Klauss, M. Nicklas, P. J. Baker, A. D. Hillier, M. Sigrist, A. Amato, and D. Johrendt, Phys. Rev. B **87**, 180503(R) (2013).
[21] K. Matano, K. Arima, S. Maeda, Y. Nishikubo, K. Kudo, M. Nohara, and Guo-qing Zheng, Phys. Rev. B **89**, 140504(R) (2014).
[22] F. Brückner, R. Sarkar, M. Günther, H. Kühne, H. Luetkens, T. Neupert, A. P. Reyes, P. L. Kuhns, P. K. Biswas, T. Stürzer, D. Johrendt, and H. H. Klauss, arXiv:1312.6166.
[23] W.-S. Wang, Y.-Y. Xiang, Q.-H. Wang, F. Wang, F. Yang, and D.-H. Lee, Phys. Rev. B **85**, 035414 (2012).
[24] Y.-Y. Xiang, W.-S. Wang, Q.-H. Wang, and D.-H. Lee, Phys. Rev. B **86**, 024523 (2012).
[25] Y.-Y. Xiang, F. Wang, D. Wang, Q.-H. Wang, and D.-H. Lee, Phys. Rev. B **86**, 134508 (2012).
[26] Y.-Y. Xiang, Y. Yang, W.-S. Wang, Z.-Z. Li, and Q.-H. Wang, Phys. Rev. B **88**, 104516 (2013).
[27] Q.-H. Wang, C. Platt, Y. Yang, C. Honerkamp, F. C. Zhang, W. Hanke, T. M. Rice, and R. Thomale, Euro. Phys. Lett. **104**, 17013 (2013).
[28] Y. Yang, W.-S. Wang, Y.-Y. Xiang, Z.-Z. Li, and Q.-H. Wang, Phys. Rev. B **88**, 094519 (2013).
[29] C. Wetterich, Nucl. Phys. B **352**, 529 (1991).
[30] See. e.g., M. Salmhofer and C. Honerkamp, Prog. Theor. Phys. **105**, 1 (2001); C. Honerkamp, M. Salmhofer, N. Furukawa, and T. M. Rice, Phys. Rev. B **63**, 035109 (2001).
[31] See. e.g., F. Wang, H. Zhai, Y. Ran, A. Vishwanath, and D.-H. Lee, Phys. Rev. Lett. **102**, 047005 (2009).
[32] P. Giannozzi, S. Baroni, N. Bonini, M. Calandra, R. Car, C. Cavazzoni, D. Ceresoli, G. L Chiarotti, M. Cococcioni, I. Dabo, A. D. Corso, S. de Gironcoli, S. Fabris, G. Fratesi, R. Gebauer, U. Gerstmann, C. Gougoussis, A. Kokalj, M. Lazzeri, L. Martin-Samos, N. Marzari, F. Mauri, R. Mazzarello, S. Paolini, A. Pasquarello, L. Paulatto, C. Sbraccia S. Scandolo, G. Sclauzero, A. P Seitsonen, A. Smogunov, P. Umari, and R. M. Wentzcovitch, J. Phys.: Condens. Matter **21**, 395502 (2009); S. Baroni, A. Dal Corso, S. de Gironcoli, P. Giannozzi, C. Cavazzoni, G. Ballabio, S. Scandolo, G. Chiarotti, P. Focher, A. Pasquarello, K. Laasonen, A. Trave, R. Car, N. Marzari, and A. Kokalj, http://www.quantum-espresso.org/.
[33] Here we use the experimental lattice parameters from Ref. [1]. We adopt the exchange correlation functional introduced by J. P. Perdew, K. Burke, and M. Ernzerhof, Phys. Rev. Lett. **77**, 3865 (1996). The wave functions are expanded by plane waves up to a cutoff energy of 60 Ry. Dense $16 \times 16 \times 8k$-point meshes are used for self-consistent calculations.
[34] N. Marzari and D. Vanderbilt, Phys. Rev. B **56**, 12847 (1997); I. Souza, N. Marzari, and D. Vanderbilt, *ibid.* **65**, 035109 (2001); A. A. Mostofi, J. R. Yates, Y.-S. Lee, I. Souza, D. Vanderbilt, and N. Marzari, Comput. Phys. Commun. **178**, 685 (2008).
[35] Notice that upon point group operations the orbitals also change. See, e.g., Y. Wan and Q.-H. Wang, Europhys. Lett. **85**, 57007 (2009).
[36] M. H. Fischer, T. Neupert, C. Platt, A. P. Schnyder, W. Hanke, J. Goryo, R. Thomale, and M. Sigrist, Phys. Rev. B **89**, 020509(R) (2014).
[37] We remark that the in-plane $\chi^{xx,yy}$ hardly change across T_c here, since the SOC is present and is much larger than the mean field pairing gap. For consistency we checked that in the limit of $\lambda \to 0$, $\chi^{xx,yy}$ for singlet pairing become identical to χ^{zz}.
[38] Jian-Xin Li, Phys. Rev. Lett. **91**, 037002 (2003).
[39] N. Bulut, D. J. Scalapino, and S. R. White, Phys. Rev. B **47**, 2742 (1993).